

# MgO–SiO<sub>2</sub> Catalysts for the Ethanol to Butadiene Reaction: The Effect of Lewis Acid Promoters

Blanka Szabó,<sup>[a]</sup> Gyula Novodárszki,<sup>[a]</sup> Zoltán Pászti,<sup>[a]</sup> Attila Domján,<sup>[b]</sup> József Valyon,<sup>[a]</sup> Jenő Hancsók,<sup>[c]</sup> and Róbert Barthos<sup>\*[a]</sup>

MgO–SiO<sub>2</sub> samples, having the composition of natural talc (NT), were obtained by co-precipitation (CP) and wet kneading (WK) methods. The materials were used as catalysts of the ethanol-to-1,3-butadiene reaction. ZnO, Ga<sub>2</sub>O<sub>3</sub> and In<sub>2</sub>O<sub>3</sub> were tested as promoters. The catalyst WK gave the highest 1,3-Butadiene (BD) yield among the non-promoted catalysts because of the high specific surface area and strong basicity. Results suggested that over the neat WK catalyst the acetaldehyde coupling to crotonaldehyde was the rate-determining process step. Forma-

tion of crotyl alcohol intermediate was substantiated to proceed by the hydrogen transfer reaction between crotonaldehyde and ethanol. The crotyl alcohol intermediate becomes dehydrated to BD or, in a disproportionation side reaction, it forms crotonaldehyde and butanol. The promoter was found to increase the surface concentration of the reactant and reaction intermediates, thereby increases the rates of conversion and BD formation. The order of promoting efficiency was Zn > In > Ga.

## 1. Introduction

Currently production of ethylene is based on the thermal cracking of naphtha. In this process 1,3-Butadiene (BD), needed for rubber manufacturing, is obtained as by-product. The developments in ethylene production technologies, such as, oxidative dehydrogenation of ethane led to BD shortage on the market. There is a need for alternative technologies for BD production. Recently the interest of both academic and industrial research renewed in the production of BD from biomass-derived feedstock.<sup>[1,2]</sup> A possible process is the bioethanol-to-BD (ETB) reaction.

Two technologies were elaborated for the production of BD from ethanol. The Lebedev-process<sup>[3]</sup> where the ethanol is converted to BD over mixed oxide catalyst, like MgO–SiO<sub>2</sub> or ZnO–Al<sub>2</sub>O<sub>3</sub>, and the process of Ostromislensky<sup>[4]</sup> where a mixture of ethanol and acetaldehyde is reacted over alumina or clay

catalysts. Recently, different oxides, mixed oxides, and zeolite supported catalysts, such as, SiO<sub>2</sub>,<sup>[5–8]</sup> SiO<sub>2</sub>–ZrO<sub>2</sub>,<sup>[9]</sup> zeolite Beta,<sup>[10]</sup> and MgO–SiO<sub>2</sub><sup>[11–26]</sup> promoted with metals and/or metal oxides, such as oxides of Zn,<sup>[8,9,17,24,25,27]</sup> Ag,<sup>[10,27,28]</sup> Cu,<sup>[10,27]</sup> Au,<sup>[11]</sup> and Ga,<sup>[15,29]</sup> and metal combinations, like Zn–Hf,<sup>[5]</sup> Zn–Ta<sup>[7,30]</sup> and Zn–Zr<sup>[13,23,26]</sup> have been reported to be active in the ETB process.


The ETB process is a set of consecutive reactions. The reaction goes through dehydrogenation of ethanol to acetaldehyde, followed aldol coupling to crotonaldehyde that has to become hydrogenated to crotyl alcohol. The alcohol is then dehydrated to BD. According to the comparative assessment of Patel et al.<sup>[31]</sup> the BD production from bioethanol can be beneficial in comparison to the petroleum-based BD production process.


Magnesia-silica mixed oxide is the most frequently used catalyst or catalyst support in the conversion of ethanol to BD. There is a general agreement that the synthesis method and the Mg to Si ratio determine the acid-base and redox properties and thereby, the hydrogenation-dehydrogenation and dehydration activity of the catalyst. The acid-base pair sites are attributed to the charge imbalance along the Mg–O–Si bonds. Pronounced formation of such sites is expected if the homogeneity of the oxide mixture is increased. Previous studies pointed out that subtle balance of acid-base and redox sites is necessary to achieve high BD selectivity.<sup>[11]</sup> The basic oxide ions of magnesia initiate the dehydrogenation and aldol addition and condensation reactions.<sup>[8,17,22]</sup> The roles of the silica component in the MgO–SiO<sub>2</sub> mixed oxides are (i) to increase the amount of crystal defects in the MgO structure, enhancing the dehydrogenation activity,<sup>[21]</sup> (ii) to increase the specific surface area (SSA) of the catalyst, (iii) to generate hydrous magnesium silicates, containing Mg–O–Si bonds showing weakly acidic character and dehydration activity. The ETB selectivity could be enhanced by bringing all these properties in the harmony, which is the best regarding the reaction.<sup>[22]</sup> The MgO–SiO<sub>2</sub> catalysts are synthesized either by wet kneading,<sup>[19–21,26]</sup> or by

[a] B. Szabó, Dr. G. Novodárszki, Dr. Z. Pászti, Prof. J. Valyon, Dr. R. Barthos  
Institute of Materials and Environmental Chemistry  
Research Centre for Natural Sciences  
Magyar tudósok körútja 2  
Budapest 1117 (Hungary)  
E-mail: barthos.robort@ttk.hu

[b] Dr. A. Domján  
NMR Laboratory  
Research Centre for Natural Sciences  
Magyar tudósok körútja 2  
Budapest 1117 (Hungary)

[c] Prof. J. Hancsók  
Institute of Chemical and Process Engineering  
University of Pannonia  
Egyetem utca 10  
Veszprém 8201 (Hungary)

 Supporting information for this article is available on the WWW under <https://doi.org/10.1002/cctc.202001007>

 © 2020 The Authors. Published by Wiley-VCH GmbH. This is an open access article under the terms of the Creative Commons Attribution License, which permits use, distribution and reproduction in any medium, provided the original work is properly cited.

co-precipitation,<sup>[14,20,22,23]</sup> and, in case, by the incipient wetness impregnation of the obtained mixed oxide by a metal oxide precursor compound.<sup>[11]</sup> The natural hydrated magnesium silicate mineral (talc) can also serve as catalyst or catalyst support.<sup>[25]</sup>

Addition of a metal/metal-oxide promoter to the MgO–SiO<sub>2</sub> significantly enhances the ethanol dehydrogenation and, as a consequence, the aldol condensation becomes the rate-determining step over the promoted catalysts. Angelici et al.<sup>[19]</sup> showed that copper additive increased the dehydrogenation activity and weakened the acidity of the catalyst. Both effects suppressed the undesired ethanol dehydration reaction to ethylene or diethyl ether, hence higher BD yields could be obtained.

Studies discuss the effect of the MgO/SiO<sub>2</sub> ratio on the BD selectivity. At low magnesia contents ethylene and diethyl ether are the main reaction products. By increasing the magnesia content the BD selectivity gradually increases. Most often volcano-type dependence was reported about the yield of BD as function of the MgO content, The maximum yield was obtained at MgO to SiO<sub>2</sub> molar ratio close to one (weight ratio 0.67).<sup>[11,12,22,24]</sup> Another study reported that the natural talc, having a MgO to SiO<sub>2</sub> molar ratio of 0.5 showed good catalytic performance in the ETB reaction.<sup>[25]</sup> In contrast, Lewandowski et al.<sup>[26]</sup> found the best activity at molar ratio 4.4 (weight ratio 3).

NMR studies of the acidity-structure relation led to adverse conclusions. Chung et al.<sup>[14]</sup> conducted NMR studies on wet-kneaded MgO–SiO<sub>2</sub> catalysts, synthesized using different magnesia sources. The BD selectivity was linked to hydrous magnesium silicates giving <sup>29</sup>Si-NMR signals in the region of –85 to –98 ppm. In contrast, Zhu et al.<sup>[32]</sup> attributed favourable activity to amorphous magnesium silicate phases, giving Si signals at –70, –75 and –92 ppm.

The XPS technique can distinguish different chemical surface environments. According to the literature, the Si and O core electron binding energies are associated primarily with the charge on the tetrahedral SiO<sub>4</sub> building blocks, reflecting the linkage of these tetrahedral.<sup>[33,34]</sup> For example, if each SiO<sub>4</sub><sup>4–</sup> unit is connected to four identical units, there is no formal charge on the tetrahedra. This structure is associated with high binding energies of both the Si 2p (103.5–104.0 eV) and the O 1s (around 533 eV) core levels.<sup>[35]</sup> If each tetrahedron shares three oxygen ions with adjacent identical tetrahedral, forming an infinite two-dimensional sheet, like in talc, then the repeating unit is Si<sub>4</sub>O<sub>10</sub><sup>4–</sup> and the formal charge on each tetrahedron is –1. As a result the Si and O binding energies are lower by about 0.5–0.6 eV. On the other extreme of scale, forsterite (Mg<sub>2</sub>SiO<sub>4</sub>) contains, independent SiO<sub>4</sub><sup>4–</sup> tetrahedra, surrounded by Mg<sup>2+</sup> cations. The charge on each SiO<sub>4</sub> unit is –4 and the corresponding Si 2p and O 1s binding energies are as low as 101.8 and 530.9 eV, respectively.<sup>[36]</sup> The pronounced shift of the Si and O photoelectron lines is accompanied by a similar but smaller shift of the Mg 2p line (from 50.7 eV in talc<sup>[33]</sup> to 50.2–50.4 eV in forsterite).<sup>[36]</sup> Another study showed that incorporation of magnesium into silica network lowers the Si binding energy into the range of 101.0–101.7 eV.<sup>[32]</sup>

As result of Si incorporation in magnesia a new peak appears in the Ultraviolet-Visible (UV-Vis) spectrum at 275 cm<sup>–1</sup>. This spectral feature was brought in relation with the catalytic activity of the MgO–SiO<sub>2</sub> catalysts in the ETB reaction.<sup>[21,37]</sup> The peak was attributed to the absorption of coordinatively unsaturated O<sup>2–</sup> ions generated by the Si, built in the magnesia structure.

The acid-base properties of MgO–SiO<sub>2</sub> catalysts are most often characterized by TPD<sup>[19,20,23]</sup> and FTIR<sup>[11,19,20]</sup> examinations of species obtained from adsorption of basic or acidic molecules. CO<sub>2</sub>-TPD and CO<sub>2</sub>-FTIR studies of Menezes et al.<sup>[38]</sup> suggested that surface heterogeneity increases the concentration of basic sites. Angelici et al.<sup>[20]</sup> showed that co-precipitated catalysts contain higher amount of acid and strong-base surface sites than those prepared by wet kneading. This finding and the increased yield of ethylene and diethyl ether by-products in the ETB reaction was explained by the better homogeneity of the co-precipitated catalyst, i. e., by the formation of many Mg–O–Si bonds.

The relation of the method and conditions of catalyst preparation, the structure and texture of the catalyst, and the ETB activity is not clearly known yet.<sup>[11,23,28]</sup> The present systematic study intends to decrease the lack of knowledge on this field. Two materials, having the same Mg to Si ratio as the natural talc (NT), were prepared by co-precipitation and wet kneading methods. The structure, texture, composition and acid-base properties of the synthesized materials (CP and WK) and the NT were thoroughly characterized and correlated with their catalytic activity in the ETB reaction. The promoting effect of Zn, Ga and In on the physico-chemical properties of the materials and on their ETB activity was also investigated.

## 2. Results and Discussion

### 2.1. Composition, texture and crystallinity

Compositional and textural characteristics of the three MgO–SiO<sub>2</sub> materials, used in the present study, are given in Table 1. The Si to Mg weight ratio of the catalysts is close to the 1.54 Si-to-Mg weight ratio in the chemical formula of natural talc (Mg<sub>3</sub>Si<sub>4</sub>O<sub>10</sub>(OH)<sub>2</sub>). Comparison of the bulk and surface compositions indicate a slight surface enrichment of Mg for the natural talc and for the co-precipitated material. This is not

**Table 1.** Characterization of the catalysts.

Catalyst	Si/Mg ratio <sup>[a]</sup>	Surface area [m <sup>2</sup> g <sup>–1</sup> ]	Pore volume <sup>[b]</sup> [cm <sup>3</sup> g <sup>–1</sup> ]	Pore diameter <sup>[c]</sup> [nm]
Natural talc	1.46 (1.40)	9.1	–	–
Co-precipitation	1.44 (1.33)	207.5	0.31	3.50
Wet kneading	1.61 (1.71)	249.6	0.76	6.40

[a] m/m, calculated from ICP-OES and XPS (in parentheses) analysis. Theoretical Si/Mg ratio is 1.54. [b] Gurvich method. [c] B.J.H. method.

surprising as the surface of most magnesium silicates tends to contain more Mg than the bulk.<sup>[36]</sup> The exception is the wet-kneaded sample, which is somewhat Mg-deficient both at the surface and in the bulk with respect to the natural talc. The SSA of the NT sample is significantly lower than that of the synthesized samples. According to the XRD and nitrogen adsorption measurements summarized in Figures 1A and B, respectively, this material is non-porous and is well crystallized. Figure 1B shows that the CP and WK samples have micro and mesoporosity.

Both samples show Type IV isotherm with H2 type hysteresis loop and another hysteresis loop at  $p/p_0 > 0.9$  due to pores among agglomerated particles. The XRD patterns evidence the low crystallinity of the CP and WK samples. A broad peak of the amorphous silica around  $2\theta$  at about  $23^\circ$  can be noticed on the diffractograms. Reflections of MgO having periclase structure is present in the XRD pattern of the WK sample ( $43.0^\circ$  and  $62.5^\circ$ ), whereas the CP sample shows broad line centered at  $35.3^\circ$  and  $61.0^\circ$  indicating the presence of an amorphous magnesium silicate phase.<sup>[11]</sup> These results suggest that the CP sample is a more homogeneous mixture of  $Mg^{2+}$  and  $Si^{4+}$  ions, while the WK sample consists of nano and microsize domains of silica and magnesia probably linked at the contacting surfaces of the two phases.

## 2.2. SEM-EDX studies

The morphology of the catalysts was studied by means of SEM-EDX equipment. The elemental map of NT and CP samples show that the Mg and Si are distributed homogeneously. Some enrichment of Mg was observed on NT sample. In contrast, the separate MgO and  $SiO_2$  phases are clearly visible in the WK sample. The NT sample shows lamellar, non-porous structure, while the CP and NT samples have flower-like structure, rich in corners and edges. Due to their low concentration (1 wt%)

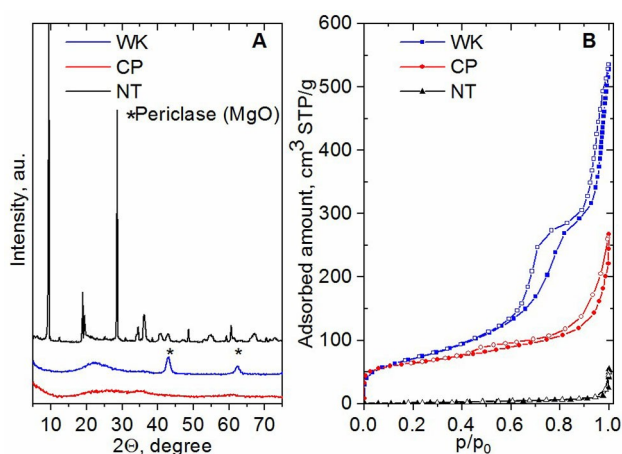


**Figure 1.** XRD patterns of (A) wet-kneaded (WK), co-precipitated (CP), and natural talc (NT) samples and (B)  $N_2$  adsorption isotherms of the samples. Adsorption and desorption branches are indicated by full and open symbols, respectively.

oxide dopants could not be identified in the images, however, the results of quantitative analysis is similar to the values determined by other methods. The images and other details are shown in Figures S1-S2.

## 2.3. NMR studies

Due to the low level of crystallization XRD could not provide adequate information about the bulk structure of the samples. Therefore,  $^1H$  MAS NMR,  $^{29}Si$  CP MAS NMR, and  $^1H$ - $^{29}Si$  FSLG HETCOR NMR spectra were recorded to evaluate the environment of the Si atoms and the possible formation of magnesium silicate phases. Figure 2A shows that all the hydroxyl groups have identical environment in the crystal structure of the NT sample resulting in a single  $^1H$  MAS NMR signal at 0.3 ppm. The relatively low chemical shift suggests that the hydroxyl groups are isolated from each other. The CP sample contains less hydrogen atoms than the NT sample. Two different signals

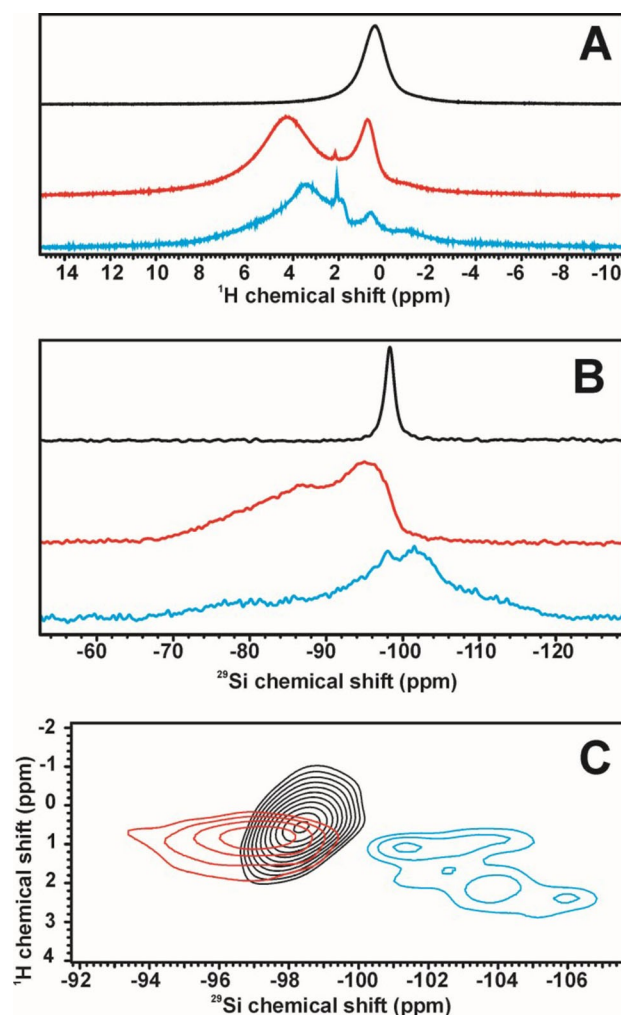


**Figure 2.** Solid state NMR spectra natural talc (NT), wet-kneaded (WK) and co-precipitated (CP) samples. (A)  $^1H$  single pulse MAS NMR spectra, (B)  $^{29}Si$  ( $^1H$ ) cross-polarization MAS NMR spectra, and (C)  $^1H$ - $^{29}Si$  FSLG HETCOR representation of the results.

could be distinguished. The signal at 0.5 ppm was assigned to "talc-like" and terminal hydroxyl groups. The broader signal at 4.1 ppm belongs most probably to H-bonded hydroxyl groups and strongly absorbed/structural water molecules. The WK sample contains even less hydrogen atoms. The signals are similar to those obtained for the CP sample, but their intensity is much lower and the broad signal has a chemical shift value of about 3.3 ppm indicating less pronounced H-bonding.

The  $^{29}\text{Si}$  CP MAS NMR chemical shift depends on the environment of the silicon atoms. The NT sample shows a single well defined signal at  $-98$  ppm (Figure 2B). Pure  $\text{SiO}_2$  has a chemical shift around  $-110$  ppm which decreases by replacing the neighboring atoms of the  $\text{SiO}_4$  tetrahedra by H or Mg. In order to get spectra, which are easier to interpret direct polarization  $^{29}\text{Si}$  spectra were recorded with relatively short relaxation delay (5 sec) to filter out the signals of pure crystalline or semi-crystalline  $\text{SiO}_2$  phases, having long  $T_1$  relaxation time. Nevertheless, the spectrum of the WK sample remained dominated by  $Q_3$  and  $Q_4$  signals of the  $\text{SiO}_2$  phase. Signal belonging to  $\text{Si}(\text{OSi})_3\text{OH}$  ( $Q_3$ ) phase was clearly shown by the  $^1\text{H}$ - $^{29}\text{Si}$  FSLG HETCOR spectrum (Figure 2C). No  $Q_4$  phase is detectable in the spectrum of CP sample (Figure 2B). According to the correlation spectra (Figure 2C), signals between  $-70$  and  $-99$  ppm originate from different magnesium hydroxy silicate species.<sup>[14,32]</sup>

## 2.4. XPS examinations

The bonding environment of Si, Mg, and O on the surface of the mixed oxide catalysts was explored by XPS. Apart from these components, XPS identified carbon in all samples, which is attributed to the adventitious hydrocarbon contamination. The CP sample contained a small amount of sodium; the concentration of all other possible contaminants remained below the detection limit of XPS.

The Mg 2p, Si 2p, O 1s, and C 1s spectra are presented as Supporting Information (Figure S3). All photoelectron peaks were adequately modeled by a single peak of symmetric shape (except the C 1s peak of the CP and WK samples). The binding energies of the Mg, Si, and O core levels for the natural talc sample showed very good agreement with the data found in the literature for talc materials.<sup>[33–35,39,40]</sup> (Cf. Supporting Information). The main results of the XPS measurements are summarized in Table 2. For the first sight it appears that the binding energy of the Mg 2p electrons are rather similar in the different samples. It is not surprising as, according to literature data,<sup>[34,35,41]</sup> the Mg binding energy, the Auger kinetic energy, and the Auger parameter values seem to overlap for many oxygen-containing magnesium compounds, such as, MgO and Mg-silicates. However, the width of the Mg 2p, Si 2p and O 1s peaks, measured for the synthetic preparations, is broader than the width of the corresponding peaks of natural talc, suggesting that the chemical environment of these components on the surface is more inhomogeneous than on the surface of natural talc. This finding is in accordance with the disordered nature of the material demonstrated also by both the XRD and NMR examinations. With respect to those in talc the Mg 2p, Si 2p, and O 1s binding energies were significantly lower for the CP sample. The Si 2p and the O 1s peaks shifted by approximately 1 eV, whereas the shift of the Mg 2p line was smaller. These results suggest increased negative charge on the  $\text{SiO}_4$  tetrahedral units, which indicates that they are significantly less interconnected than in talc.<sup>[33–36]</sup>

The Mg 2p, Si 2p, and O 1s binding energies of the WK sample are intermediate between those of the NT and the CP samples. The peaks are broader than either in the CP or the NT samples, indicating that this material has the most inhomogeneous structure. The XRD studies revealed the presence of MgO crystallites, whereas the results of NMR showed the formation of hydrated  $\text{SiO}_2$  ( $Q_3$ ) in the material. Nevertheless, the broad and smooth character of the XPS peaks did not permit their

**Table 2.** XPS results for the natural talc (NT), the co-precipitated (CP) and the wet-kneaded (WK) materials.

Sample	Composition at [%]	Mg:Si	Binding energies, Auger kinetic energies, Auger parameters (eV) <sup>[a]</sup>								
			Mg 2p	Mg 1s	Mg KLL	Mg AP <sup>[b]</sup>	Si 2p	Si KLL	Si AP <sup>[c]</sup>	O 1s	C 1s <sup>[d]</sup>
NT	Mg: 16.7 Si: 20.3 O: 60.8 C 2.2	3.29:4	50.7 (2.1)	1304.4	1179.7	2484.1	103.4 (2.1)	1608.5	1711.9	532.5 (2.4)	285.0
CP	Mg: 15.2 Si: 17.4 O: 56.2 C: 9.6 Na: 1.7 <sup>e</sup>	3.49:4	50.2 (2.2)	1304.0	1180.0	2484.0	102.4 (2.5)	1609.4	1711.6	531.7 (2.9)	285.0 288.6 <sup>f</sup>
WK	Mg: 13.7 Si: 20.3 O: 59.6 C: 6.4	2.70:4	50.5 (2.8)	1304.3	1179.9	2484.2	102.8 (2.6)	1608.7	1711.5	532.1 (3.0)	285.0 290.6 <sup>g</sup>

[a] Values in parentheses under the binding energy values indicate the full width at half maximum (FWHM, in eV) of the fitting Gaussian-Lorentzian product curve. [b] Mg Auger parameter: sum of the binding energy of the Mg 1s photoelectron peak and the kinetic energy of the Mg  $\text{KL}_{23}\text{L}_{23}$  Auger peak. [c] Si Auger parameter: sum of the binding energy of the Si 2p photoelectron peak and the kinetic energy of the Si  $\text{KL}_{23}\text{L}_{23}$  Auger peak (excited by Bremstrahlung from the Al X-ray anode). [d] The main component of the C 1s spectrum arising from hydrocarbons was used for charge compensation. [e] Na 1s binding energy: 1072.2 eV, Na KLL Auger kinetic energy: 988.6 eV, Na Auger parameter: 2060.8 eV, all pointing to  $\text{Na}^+$  ions in a silicate and/or glass environment. [f] Small contribution, assigned to carboxylic groups [e.g. NIST data base. [g] Minor contribution, assigned to carbonates.



reliable resolution into component peaks. The Si Auger parameter at 1711.5 eV is clearly below the narrow range around 1712 eV, usually reported for silicates or crystalline SiO<sub>2</sub>. Latter finding substantiates the presence of a gel-like silica, i.e., strongly hydrated SiO<sub>2</sub> component.<sup>[33]</sup> It is plausible that the bulk-sensitive XRD and NMR and the surface-sensitive XPS measurements reveal different features of this sample. While the bulk-sensitive techniques indicate the presence of MgO- and SiO<sub>2</sub>-like regions, the XPS data can be interpreted as indication of formation of interfacial Si–Mg mixed oxide between the SiO<sub>2</sub> and MgO domains and on the surface of the particles. It was shown before that in systems prepared by MgO deposition onto clean or oxidized Si surface or by Mg deposition onto SiO<sub>2</sub> surface, an interfacial disordered Mg-silicate layer was formed during annealing.<sup>[42,43]</sup> Obviously, a mixed Si–Mg oxide phase is more favored by thermodynamics than the coexistence of separate MgO and SiO<sub>2</sub> phases. Such intermixing could be initiated by the 500 °C calcination of the WK material. Under these circumstances the surface of the WK sample should contain not only SiO<sub>2</sub> and MgO domains but also certain amounts of disordered Mg-silicates, which is in line with the high extent of inhomogeneity, suggested by the XPS results. A particular feature of the WK sample is the rather strong high binding energy C 1s peak around 290.6 eV, which appears in addition to the common hydrocarbon-related carbon peak. The intensity of this peak amounts to about 25% of the total C signal intensity (Figure S3D). The high binding energy indicates the presence of highly oxidized, carbonate-like carbon species.<sup>[36,41]</sup> It may be noted that while such carbonate contributions are rarely observed on silica surfaces, they readily form on MgO exposed to CO<sub>2</sub>-containing ambient.<sup>[44]</sup> The appearance of the carbonate signal for the WK sample and its lack for the NT and CP samples confirm that the former indeed contains MgO-like surface regions.

## 2.5. TPD and FTIR characterization of the acid-base properties

There is agreement in the literature that the acid-base properties of catalysts play a key role in the ETB reaction. For characterization of acid-base properties we should know the number, strength, and strength distribution of the acid and base sites. The most commonly used methods characterize is the adsorption of acidic or basic probe molecules on the catalyst surface. Usually some spectral change of the adsorbed probe is determined, or the strength of the adsorption is related

to the thermal stability of the adsorbed species. The use of probe molecules raises several issues: (i) the acidity/basicity of the probe molecule delimits the sites that can be characterized, (ii) the adsorption interaction changes the acid-base properties of the catalyst, (iii) shape and size selective adsorption inhibitions may occur, (iv) the stoichiometry of the adsorption is not always unequivocal, etc.. In the present study TPD patterns of NH<sub>3</sub> and CO<sub>2</sub>, as well as, FTIR spectra of adsorbed CDCl<sub>3</sub> and Py were determined and evaluated to characterize the acid-base properties of the catalysts. Results derived from the TPD curves shown in Figures S4 and S5 are summarized in Table 3. The smallest amounts of adsorbed CO<sub>2</sub> and NH<sub>3</sub> were measured for the NT sample, which can be explained by the very low surface area of the mineral. The WK sample has higher CO<sub>2</sub> uptake than the CP sample, whereas their NH<sub>3</sub> uptakes is similar. The higher CO<sub>2</sub> uptake suggests that the WK sample is more basic than the CP sample. This can correspond to the presence of MgO domains in the former sample, as suggested by the XPS data.

The dopant ZnO had virtually no effect on the acid-base properties of the NT sample. The corresponding properties of the In<sub>2</sub>O<sub>3</sub> and Ga<sub>2</sub>O<sub>3</sub> doped NT sample were not tested. It is noteworthy that the additives approached the CO<sub>2</sub> uptake of the catalysts, i.e., the basicity of the CP and WK catalysts approached to each other. The addition of metal oxides significantly increased the ammonia uptake, i.e., acidity of the catalysts. The Ga/CP sample was an exception. In this series of measurements it could be observed that the addition of metal oxide dopant brought the ammonia uptake of the samples almost to the same level (Table 3).

The order of basicity of the neat MgO–SiO<sub>2</sub> samples is also supported by the CDCl<sub>3</sub> adsorption measurements shown in Figure 3A. The presented spectra do not show bands at 2139 and 2086 cm<sup>-1</sup>, which Angelici et al.<sup>[20]</sup> assigned to CDCl<sub>3</sub>, bound to strong basic sites. The spectra in Figure 3A are more similar to those reported by Paukshtis et al.<sup>[45]</sup> in their pioneering work. The ν<sub>CD</sub> frequency of free CDCl<sub>3</sub> molecules is at 2260 cm<sup>-1</sup>. Interaction of CDCl<sub>3</sub> molecules and basic surface sites shifts the ν<sub>CD</sub> stretching band to lower wavenumbers.<sup>[20,45]</sup> The band displacement reflects the strength of interaction and, thereby, the base strength of the adsorbing surface sites. The integrated band area gives an approximate measure of the amount of adsorption sites. Figure 3A shows that the WK sample contains the highest number of basic sites, whereas the NT sample of low surface area has only small amount of similar sites. This is in accordance with the results of the CO<sub>2</sub>-TPD study. Unlike the

**Table 3.** Results of CO<sub>2</sub> and NH<sub>3</sub> Temperature Programmed Desorption (TPD) measurements. Natural talc (NT), Co-precipitated sample (CP), Wet-kneaded sample (WK).

Catalyst	Support C <sub>basic</sub> <sup>[a,b]</sup>	C <sub>acidic</sub> <sup>[a,c]</sup>	1% Ga <sub>2</sub> O <sub>3</sub> C <sub>basic</sub> <sup>[a,b]</sup>	C <sub>acidic</sub> <sup>[a,c]</sup>	1% In <sub>2</sub> O <sub>3</sub> C <sub>basic</sub> <sup>[a,b]</sup>	C <sub>acidic</sub> <sup>[a,c]</sup>	1% ZnO C <sub>basic</sub> <sup>[a,b]</sup>	C <sub>acidic</sub> <sup>[a,c]</sup>
NT	7.7	17.1	n.m. <sup>[d]</sup>	n.m. <sup>[d]</sup>	n.m. <sup>[d]</sup>	n.m. <sup>[d]</sup>	7.3	15.6
CP	10.5	412.0	22.7	394.0	27.3	735.1	19.2	693.7
WK	94.5	461.1	52.2	910.2	45.5	933.2	34.8	879.5

[a] Concentrations in μmol/g units. [b] Adsorption of CO<sub>2</sub> at 13 kPa and room temperature, flushed for 15 min, evacuated, then ramped up in He flow at a rate of 10 °C min<sup>-1</sup> to 500 °C and held at this temperature for 1 h. [c] Same procedure by using 13 kPa NH<sub>3</sub>. [d] Non measured.

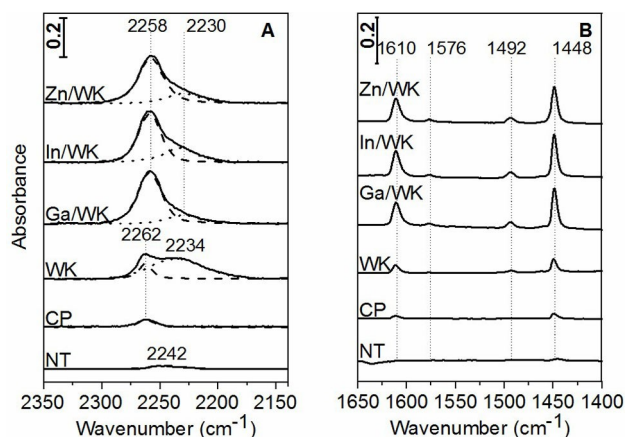


**Figure 3.** FTIR spectra of adsorbed (A)  $\text{CDCl}_3$  and (B) pyridine. The pellets were pre-treated in vacuum at  $450^\circ\text{C}$  for 1 h. The spectra were recorded at room temperature (A) in the presence of  $\text{CDCl}_3$  at about 933 Pa pressure, and (B) after adsorption of pyridine at 666 Pa pressure at  $200^\circ\text{C}$  and evacuation at the same temperature for 30 min.

spectra of the NT and CP samples the FTIR spectrum of the WK sample exhibits two  $\nu_{\text{CD}}$  component peaks, suggesting the presence of two kinds of adsorption sites having different base strengths (Figure 3A). The broad band at  $2234\text{ cm}^{-1}$  indicates the presence of sites having stronger basicity than the sorption sites of the other samples. The adsorption of  $\text{CO}_2$  on these sites can be responsible for the pronounced tailing of the  $\text{CO}_2$ -TPD peak at its high-temperature side (Figure S4C). Figure 3A shows that addition of metal oxide significantly decreased the relative and absolute amounts of strong base adsorption sites. While the total peak area increased only slightly, the area ratio of the peaks at about  $2230$  and  $2260\text{ cm}^{-1}$  changed significantly. The ratio that was 4.94 for the WK sample dropped to 0.42, 0.30, and 0.21 for the In/WK, Zn/WK and Ga/WK samples, respectively. It is clear that the additive decreased the basicity of the WK catalysts.

Vibrations of the aromatic ring of adsorbed Py molecules can be used to distinguish Py, coordinatively bonded to Lewis acid sites or to Brønsted acid sites in protonated form, ( $\text{PyH}^+$ ) (Figure 3B). The band, diagnostic for  $\text{PyH}^+$  should appear at about  $1545\text{ cm}^{-1}$ . The  $\text{MgO-SiO}_2$  catalysts did not have Brønsted acid sites, strong enough to protonate Py. The infrared adsorption band of pyridine bound to Lewis acid sites is around  $1445\text{ cm}^{-1}$ . Comparing the spectra of Py bound to neat  $\text{MgO-SiO}_2$  samples after identical sample treatments, it can be concluded that the NT sample does not bind any Py under the experimental conditions used, whereas the WK sample can bind and retain slightly more Py than the CP sample (Figure S4A). Figure 3B shows that addition of only 1 wt.% dopant significantly increases the Py uptake of the WK sample and also increases its Py bonding strength. Based on the thermal stability of the Py species giving the band at  $1445\text{ cm}^{-1}$ , the following order of acidity can be established:  $\text{In/WK} > \text{Zn/WK} > \text{Ga/WK}$  (Figure 3B). The spectra of the entire series of experiments and the integrated absorbance values of selected peaks are summarized in Figure S6 and Table S2.

## 2.6. ETB activity and selectivity

The initiation step of the ETB process is the dehydrogenation of ethanol to acetaldehyde. It is generally believed that the hydrogen formed during the dehydrogenation of ethanol hydrogenates the crotonaldehyde, formed from the acetaldehyde by aldol coupling, to get the crotyl alcohol intermediate of BD formation. Our results (vide infra) supports the idea that the formation of the unsaturated alcohol takes place predominantly by hydrogen transfer between ethanol and crotonaldehyde according to the Meerwein-Ponndorf-Verley (MPV) mechanism to give acetaldehyde side product. Regarding the ETB reaction the MPV process is favourable compared to the direct hydrogenation by  $\text{H}_2$  because it is highly selective in the reduction of the carbonyl group and leaves the double bond untouched. Moreover, the process generates acetaldehyde from the reducing reactant ethanol, which aldehyde can then participate then in the aldol coupling reaction step of the ETB process. The heterogeneous MPV process can take place either on Lewis acidic<sup>[46]</sup> or basic sites.<sup>[8,47–49]</sup> Niiyama et al.<sup>[48]</sup> found that over  $\text{MgO-SiO}_2$  catalysts the basic sites are responsible for the MPV activity of the ethanol. Ordonsky et al.<sup>[50]</sup> compared the activity of  $\text{ZnO}_2/\text{SiO}_2$  and  $\text{MgO/SiO}_2$  catalysts in acetaldehyde condensation and found that over  $\text{ZnO}_2$  containing catalyst the initial acetaldehyde conversion is somewhat higher. Over  $\text{MgO-SiO}_2$  catalysts the aldol condensation step is considered to take place on an acid-base pair sites by concerted mechanism.<sup>[16]</sup> Nevertheless, the catalyst of the one-step Lebedev-process must have also hydrogenation-dehydrogenation activity (Figure 4).

Obviously, the MPV reaction gives less acetaldehyde than needed to maintain the reaction. Thus, the dehydrogenation activity of the catalyst has not only to initiate the reaction, but also has to maintain high enough concentration of acetaldehyde intermediate. In this respect the use of ethanol-acetaldehyde mixture as reactant makes the dehydrogenation function of the catalyst of secondary importance.

Figure 5 shows the catalytic performance of neat  $\text{MgO-SiO}_2$  preparations in the ETB transformation. As function of temperature the conversion over the CP and WK catalysts was quite similar. The NT catalyst, having much lower surface than latter catalysts, was much less active. Over each of the catalysts the main reaction products were diethyl ether at lower temperatures, and ethylene at higher temperatures. This temperature dependence is understandable regarding that the bimolecular dehydration of ethanol is exothermic, whereas the monomolecular reaction is endothermic. The best performing ETB catalyst was the WK sample having BD selectivity around 30% in almost the whole examined temperature region. The data in

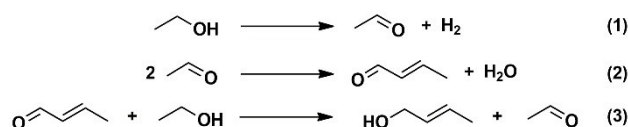


**Figure 4.** Formation of crotyl alcohol in the ETB process.

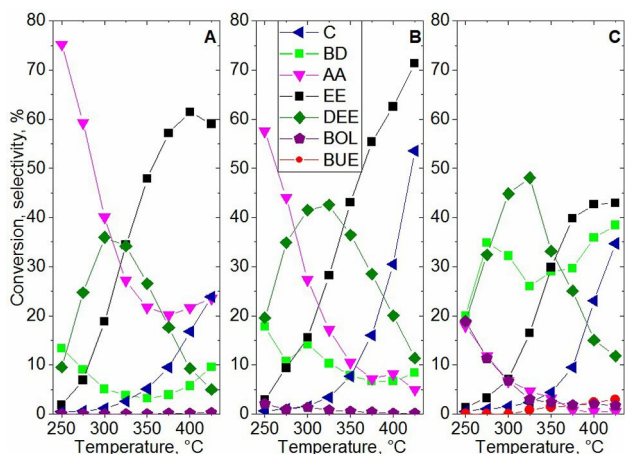


**Figure 5.** Conversion of ethanol over (A) natural talc, (B) co-precipitated, and (C) wet-kneaded MgO–SiO<sub>2</sub> catalysts as function of reaction temperature. The WHSV was 0.5 g<sub>ethanol</sub>g<sub>cat</sub><sup>-1</sup>h<sup>-1</sup> at a total gas flow rate of 30 cm<sup>3</sup> min<sup>-1</sup>. The partial pressure of ethanol was about 15 kPa in He. The conversion curve is labelled with letter C. Selectivity curves are given for butadiene (BD), acetaldehyde (AA), ethylene (EE), diethyl ether (DEE), butanol (BOL) and butanes (BUE).

Tables 3, S1, and S2 show that this catalyst has the strongest basic properties and that the number and strength of Lewis acid sites on it are also higher than those of the other two samples. The favourable catalytic activity of the WK sample is most probably due to cooperation of relatively strong basic and acidic sites on its surface.

Figures 5A and B show that especially at low temperatures the acetaldehyde was the main reaction product over the NT and CP catalysts, poorly performing in the ETB reaction. The high acetaldehyde selectivity is associated with a low yield of C<sub>4</sub> products. This suggests that over these two catalysts the aldehyde coupling catalytic function is weak. Besides generating BD, the WK catalyst also initiates formation of butanol and butenes in significant amounts, confirming that this catalyst is highly active in aldol coupling and dehydration reactions. This activity can be attributed to the strong basicity of this catalyst (Table 3).

In accordance with other studies the presumed intermediates of BD formation, such as, 3-hydroxybutanal, crotonaldehyde, and crotyl alcohol are absent or appear only in negligible amounts even at very low space times (Figures 5–7). The transformation of crotyl alcohol to BD is facile over each catalyst explaining the absence of crotonaldehyde and crotyl alcohol in the product mixtures. The high activity of the WK catalyst in converting crotonaldehyde to crotyl alcohol intermediate and C<sub>4</sub> products makes the WK preparation to the most active ETB catalyst.

Interestingly, butanol was a side product that appeared in clearly detectable amount (Figures 5–7) according to Scalbert et al.<sup>[51]</sup> the crotyl alcohol can be hydrogenated to butanol or dehydrated to BD depending on the reaction conditions and the properties of the used catalyst.

In order to better understand the formation and transformation processes of C<sub>4</sub> intermediates, we studied the

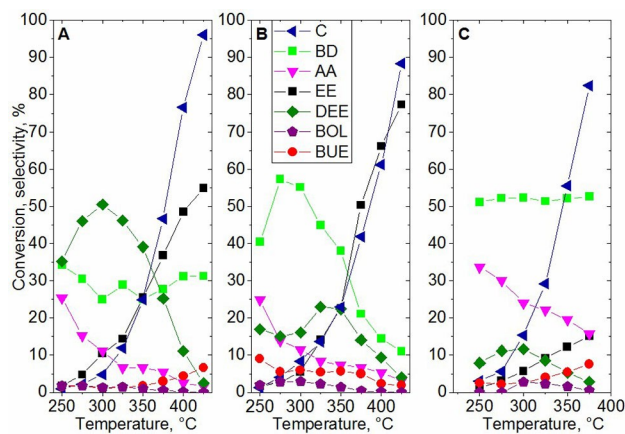


**Figure 6.** Effect of 1 wt.% (A) Ga<sub>2</sub>O<sub>3</sub>, (B) In<sub>2</sub>O<sub>3</sub>, and (C) ZnO promoter on the conversion of ethanol to butadiene. The WHSV was 0.5 g<sub>ethanol</sub>g<sub>cat</sub><sup>-1</sup>h<sup>-1</sup> at a total gas flow rate of 30 cm<sup>3</sup> min<sup>-1</sup>. The partial pressure of ethanol was about 15 kPa in He. See the Figure 5. for the legends.

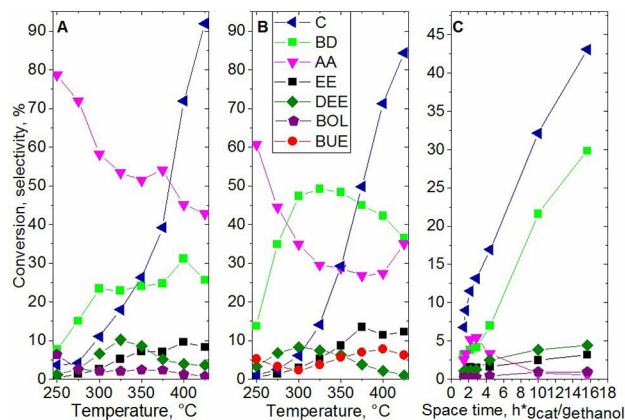


**Figure 7.** Effect of 1 wt.% ZnO additive on the activity and selectivity of (A) NT and (B) CP samples in the ETB reaction. The WHSV was 0.5 g<sub>ethanol</sub>g<sub>cat</sub><sup>-1</sup>h<sup>-1</sup> at a total gas flow rate of 30 cm<sup>3</sup> min<sup>-1</sup>. The partial pressure of ethanol was about 15 kPa in He. Section C shows the effect of WHSV on the product yield and conversion over 1 wt.% ZnO/WK sample at 300 °C, and ethanol partial pressure of about 15 kPa. The total flow rate was varied in the 5–120 cm<sup>3</sup> min<sup>-1</sup> range. See the Figure 5. for the legends.

reaction of crotyl alcohol over unpromoted MgO–SiO<sub>2</sub> catalysts (Figure 8). Full conversion was reached at around 325 °C. Over each catalyst the main reaction products were BD, formed by crotyl alcohol dehydration, and butanol. Interestingly, crotonaldehyde was also obtained. The highest amount of crotonaldehyde was obtained over the NT catalyst probably because this catalyst was hardly active in its further conversion. It cannot be excluded that butanol formation could happen by hydrogenation of crotyl alcohol consuming the hydrogen evolved in aromatization side process. GC-MS measurements showed traces of C<sub>8</sub> aromatics, such as, xylenes and styrene, were formed in low-temperature reactions. The results, obtained studying the crotonaldehyde conversion, did not support this notion. In the reaction over neat MgO–SiO<sub>2</sub> preparations formation of polyolefins and aromatics poisoned the catalysts

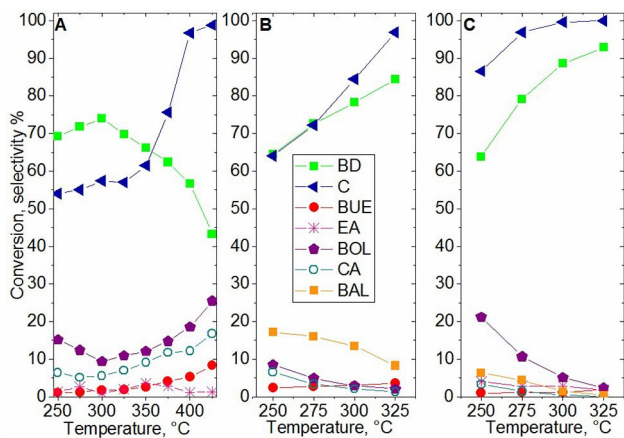


**Figure 8.** Catalytic conversion of crotyl alcohol over (A) NT, (B) CP, and (C) WK catalysts. The WHSV was  $0.125 \text{ g}_{\text{alcohol}} \cdot \text{g}_{\text{cat}}^{-1} \text{ h}^{-1}$  at a total gas flow rate of  $30 \text{ cm}^3 \text{ min}^{-1}$ . The partial pressure of crotyl alcohol was about 4 kPa in He. See the Fig.5. for the legends. CA = crotonaldehyde and BAL = butanal.

very quickly. Addition of hydrogen to the reactant did not stop rapid poisoning. It was observed that butanol and crotonaldehyde were obtained together with similar selectivities. Results seem to support that disproportionation of crotyl alcohol (Figure 9) could have been responsible for the butanol formation during the ETB process and not a direct crotonaldehyde hydrogenation.

Figure 6 shows that the conversion of ethanol and the selectivity of BD formation were significantly increased by all three applied metal oxide additives. Because the WK catalyst showed the best activity in the ETB reaction the promoting effect of Ga-, In-, and Zn-oxide was investigated using this material as support. In general, the In and Zn promoters suppressed dehydration reactions and increased both ethanol conversion and BD selectivity (Figure 6). The Ga changed only the conversion, but the product selectivities were very similar to those obtained using the non-promoted WK sample. The positive effect of In dopant is significant at temperatures 250–350 °C. The Zn/WK performs about 50% BD selectivity in the 250–375 °C temperature range. At higher temperatures the full analysis was difficult because a number of different  $\text{C}_5$ – $\text{C}_8$  dienes, trienes, and aromatics were formed.

The addition of Zn to NT remarkably suppressed the formation of ethylene and diethyl ether. The selectivity of BD formation was not affected by this dopant. However, the ethanol conversion to acetaldehyde was significantly higher than over the bare support, suggesting that dehydrogenation was promoted but the formed acetaldehyde hardly took part in the aldol coupling reaction. Addition of ZnO to the CP sample resulted in a remarkably increase of ethanol conversion and BD selectivity, while the selectivity for the dehydration products remained close to or below 10%. This result suggests that the

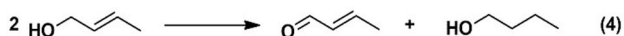


**Figure 9.** Disproportionation reaction of crotyl alcohol.

rate controlling step of ETB reaction over the CP catalyst could have been the step of ethanol dehydrogenation to acetaldehyde. Unlike to the Zn/NT catalyst, the aldol coupling activity of the Zn/CP catalyst was sufficient to bring the reaction further and get BD. Figure 7 C shows the effect of space time on the conversion of ethanol and the yield of the products over the 1% ZnO/WK catalyst. The yield of acetaldehyde passed through maximum indicating that it was a primary product that was further converted in secondary aldol condensation reaction.

There is evidence in the literature that ZnO is able to bind heterolytically dissociated hydrogen on its surface.<sup>[52]</sup> However, our attempt to detect activated hydrogen on any of our catalysts was unsuccessful. It has also been shown (vide ultra) that molecular hydrogen is unable to hydrogenate crotonaldehyde under the reaction conditions used. This is strong evidence that the crotyl alcohol intermediate of the ETB reaction could have been formed from crotonaldehyde by the MPV mechanism over our catalysts.

In our opinion, the positive effect of the metal oxide dopants on the ETB reaction cannot be directly related to the induced changes in the acid-base properties of the catalysts and to the enhanced dehydrogenation activity. It is obvious that  $\text{Zn}^{2+}$ ,  $\text{In}^{3+}$  and  $\text{Ga}^{3+}$  cations are stronger Lewis acids than  $\text{Si}^{4+}$  and  $\text{Mg}^{2+}$  cations. Stronger Lewis acid sites necessarily generate stronger Lewis base site  $\text{O}^{2-}$  anions. The adsorption measurements clearly demonstrated that the additive oxides significantly enhanced both the acidity and basicity of the catalysts. Higher ethanol conversions and higher product formation rates over doped samples can be explained by the increased surface concentration of the reactant and the reaction intermediates.

The increasing aldehyde concentration as function of space time (Figure 7C) must be paralleled by an increasing surface concentration of the aldehyde activated for aldol coupling, most probably in the form of surface enolate.<sup>[53]</sup>

The rate of aldol coupling increases with increasing space time but it remains the rate-controlling process step (Figure 7C). The steady-state product composition varies as the concentration of the surface species changes with the conversion. Figure 10 shows the product distribution over CP supported metal oxide catalysts at conversion levels of 10 to 50%. The results show that higher  $\text{C}_4$  and BD selectivities were achieved in all cases at higher conversions, i.e., at longer space times.

In general the applied metal additives were found to increase the activity and modify selectivity (Figure 10). The dopant increased not only the number active sites but also the rate constants of the different reactions. As a consequence the concentration of surface intermediates can increase and the relative amounts of the surface intermediates of different products can change. The composition of the product mixture changes accordingly. We needed each rate and adsorption equilibrium constant ( $k$  and  $K$ ) and the temperature dependence of these constants to give full description of the complex network and give the activation energy ( $E_a$ ) of each reaction. Wang et al.<sup>[17]</sup> made an attempt to determine the activation energy of the ethanol conversion and the formation of the



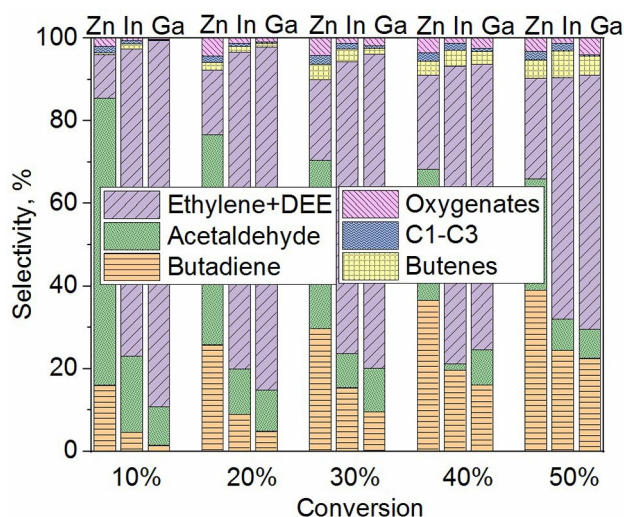


**Figure 10.** Effect of the ethanol conversion on the distribution of the reaction products over doped CP samples, doped by 1 wt.% Zn, In, or Ga-oxide doped. The reaction temperature was 350 °C, the WHSV was varied in the 0.2–1.0  $\text{g}_{\text{alcohol}} \text{g}_{\text{cat}}^{-1} \text{h}^{-1}$  range. The partial pressure of ethanol in He was about 8 kPa. Over ZnO/CP the low conversion levels were achieved by diluting of 0.50 g catalyst with 0.50 g inert SiC.

main products over MgO–SiO<sub>2</sub> and Zn/MgO–SiO<sub>2</sub> catalysts. The reported Arrhenius plots suggest that all the reactions were handled as processes of zero order kinetics. In this case only the apparent rate constants ( $k_{\text{app}}$ ) are equal with the initial rate of the reaction that can be experimentally determined. Anyhow, the obtained  $k_{\text{app}}$  includes the intrinsic  $k$  values of all the processes that contribute to forming and consuming the surface intermediate of a transformation and determines its concentration. Obviously, no strong mechanistic conclusions can be established on the values of the apparent activation energies ( $E_{\text{app}}$ ), derived from such Arrhenius plots. Getting deeper knowledge of complex reaction networks like the ETB reaction requires theoretical and microkinetic analysis.

The metal additive promotes the ethanol dehydrogenation activity. If this activity change is not paralleled by increased aldol condensation activity acetaldehyde intermediate accumulate on the surface and appears in the product mixture in higher concentration. This phenomenon was demonstrated by the study of Pomalaza et al.<sup>[30]</sup> The metal oxide additives, used in present study, had the positive effect on the BD yields in the order Zn > In > Ga.

The outstanding promoting effect of ZnO is thought to be related to its electronic structure. According to the HSAB (Hard and Soft Acids and Bases) theory, on the scale of soft and hard ions, Zn<sup>2+</sup> belongs to the borderline group, while the other two cations, as well as, the Si<sup>4+</sup> and Mg<sup>2+</sup> ions, belong to the group of hard Lewis acids.<sup>[54,55]</sup> Hayashi et al.<sup>[39]</sup> based on experimental and computational results suggested that chemical hardness is one of the chemical descriptors, which permit to predict the effect of dopant on the ETB activity of MgO–SiO<sub>2</sub> catalysts. The softness of Zn<sup>2+</sup> ion seems to be favourable regarding the BD selectivity of the catalysts at lower temperatures, whereas at

higher temperatures it promotes formation of polyolefins and aromatics.

It is also interesting, that the ZnO additive suppresses ethanol dehydration, nevertheless dehydration selectivity increases with increasing conversion. With increasing conversion the dehydration activity of the In<sub>2</sub>O<sub>3</sub> and Ga<sub>2</sub>O<sub>3</sub> doped catalysts changes in the opposite direction. Obviously the distribution of the ethanol conversion between dehydration and dehydrogenation depends both on the catalyst properties and the level of conversion.

### 3. Conclusion

Natural talc and two MgO–SiO<sub>2</sub> catalysts, having the same Mg/Si ratio as the natural talc, but synthesized in different ways, such as, co-precipitation and wet kneading, were tested in the ethanol-to-butadiene (ETB) reaction. The effect of ZnO, In<sub>2</sub>O<sub>3</sub> and Ga<sub>2</sub>O<sub>3</sub> dopants was also investigated. Examination of the neat mixed oxide catalysts showed that the catalytic activity of natural talc was low. This can be related to its non-porous structure and low specific surface area. The highest BD yields were found over the wet-kneaded catalyst. Since the acidity of the samples was similar but their basicity was much different, the highest ETB activity was attributed to the highest basicity of the catalyst prepared by wet kneading. It was shown that the catalyst prepared by wet kneading is inhomogeneous on the nano and microscale. It contains silica and strong base magnesia domains bound by Si–O–Mg bonds. Doping by metal oxide increased the acidity of the synthetic catalysts to about the same level. The basicity and the activity of the preparations were modified to different extents. The increased catalytic activity was explained by the increased concentration of the reactant/intermediate on the catalysts surface, while the differences in product distributions were interpreted by the chemical difference of the metal oxides. The oxide dopants enhanced the BD yields in the order Zn > In > Ga. Investigation of the reaction of C<sub>4</sub> intermediates suggested that the crotonaldehyde hydrogenation step in the reaction chain, giving crotyl alcohol took place according to the MPV reduction mechanism. Parallel to crotyl alcohol dehydration to BD the disproportionation of the alcohol to butanol and crotonaldehyde also proceeded.

### Experimental Section

Natural talc (Tital VT) was obtained from Sibelco Specialty Minerals Europe, The Netherlands. This material contains Fe-, Mg- and Ca-oxide impurities in low amount (<0.25 wt.%).

Two solutions were made to synthesize the CP preparation: in 400 mL methanol 52.7 g Mg(NO<sub>3</sub>)<sub>2</sub> (Sigma-Aldrich, 99%), and in 100 mL methanol 55.5 g tetraethyl orthosilicate TEOS (>98% Fluka AG) was dissolved. The mixture of the two solutions was dropwise added to 1 M NaOH solution under vigorous stirring. The pH of the mixture was maintained at 10.5 ± 0.2 by continuously adding to it the needed amount of 1 M NaOH solution. The obtained suspension was aged for 1 week at room temperature then it was repeatedly centrifuged and washed with deionized water. The pH

of the last supernatant reached the value of 7.0. The separated gel was dried at 120 °C overnight and calcined at 500 °C for 5 h.

Two gels were made and mixed to get catalyst WK. To get the first gel a solution was made by dissolving 51.28 g  $\text{Mg}(\text{NO}_3)_2$  in 200 mL ion-free water than the pH of the solution was adjusted to 12.0 by adding to it 0.5 M NaOH solution dropwise. A suspension was obtained that was aged overnight at room temperature. It was then centrifuged to separate the precipitate and washed with deionized water until the pH of the supernatant reached 7.0. The washed gel was dried at 120 °C overnight. The second gel was prepared adding dropwise 41.6 g TEOS to 440 mL of 1.5 M  $\text{NH}_3$  solution under vigorous stirring at 70 °C. The obtained gel was washed and dried at 120 °C overnight. In 100 mL deionized water 5.8 g of the first dried gel ( $\text{Mg}(\text{OH})_2$ ) and 8.0 g of the second dried gel ( $\text{SiO}_2$ ) were mixed and stirred at room temperature for 5 h (wet kneading). The solid was then separated, dried at 120 °C overnight, and calcined in air at 500 °C for 5 h. The Si to Mg weight ratio of the prepared samples was adjusted to about 1.54 that is similar to that of the natural talc. The impregnation of the MgO– $\text{SiO}_2$  preparations were executed by 33 mmol  $\text{dm}^{-3}$  solutions of  $\text{Zn}(\text{NO}_3)_2 \cdot 6\text{H}_2\text{O}$  (Fluka  $\geq 99\%$ ),  $\text{In}(\text{NO}_3)_3 \cdot x\text{H}_2\text{O}$  (Sigma Aldrich  $\geq 99.99\%$ , or  $\text{Ga}(\text{NO}_3)_3 \cdot x\text{H}_2\text{O}$  (Sigma Aldrich  $\geq 99.9\%$ ) in the amount to obtain catalysts containing about 1 wt.% of metal oxides.

The ICP-OES measurements with a simultaneous plasma emission spectrometer (Spectro Genesis) and axial plasma observation were used to determine the elemental composition of the samples.

X-ray diffraction patterns were recorded by a Philips PW 1810/3710 diffractometer using monochromatized  $\text{CuK}\alpha$  ( $\lambda = 0.15418$  nm) radiation (40 kV, 35 mA) and proportional counter. The patterns, recorded at ambient temperature, were collected between 3° and 75°  $2\theta$  range in 0.02° steps, in each step for 0.5 s.

The nitrogen adsorption/desorption isotherms of the samples were recorded at –196 °C using Thermo Scientific Surfer automatic, volumetric adsorption analyser. Prior the measurements the samples were activated under vacuum at 250 °C for 120 minutes.

A computer controlled flow-through TPD system, equipped with a U-tube (I.D. 4 mm) quartz reactor and thermal conductivity detector (TCD), was used to determine  $\text{NH}_3$  and  $\text{CO}_2$  uptakes under conditions permitting comparison of the results. (For experimental details cf. the legends of Figures. S4 and S5.)

Solid state Magic Angle Spinning Nuclear Magnetic Resonance (MAS NMR) spectra of samples were recorded by Varian System spectrometer, operating at 400 MHz for the  $^1\text{H}$  frequency, with a Chemagnetics 4.0 mm narrow-bore double resonance T3 probe. To get  $^{29}\text{Si}$  Cross Polarization Magic Angle Spinning (CP MAS) spectra 8000 transients were recorded using SPINAL-64 decoupling with 1 ms contact time, and 20 sec recycle delay. Polydimethylsiloxane (PDMS) was used as external chemical shift reference (0.21 ppm for the  $^1\text{H}$  and 0 ppm for the  $^{29}\text{Si}$  scale) The 90° pulse lengths were 5.4  $\mu\text{s}$  for  $^{29}\text{Si}$  and 2.9  $\mu\text{s}$  for the proton channel. For obtaining the  $^1\text{H}$ - $^{29}\text{Si}$  FSLG HETCOR (Frequency-Switched Lee-Goldburg Heteronuclear Correlation) spectra 384 transients were recorded with 64 increments in the  $t_1$  dimension with 10 sec recycle delay. The FSLG scaling factor was 0.53. The measuring temperature was 18 °C, the spinning rate of the rotor was 12 kHz in all measurements.

X-ray photoelectron spectra were recorded by an EA 125 electron spectrometer (OMICRON Nanotechnology GmbH, Germany). Non-monochromatic  $\text{AlK}\alpha$  radiation (1486.6 eV) was used as excitation source. Calibration of the energy scale of the instrument was checked according to the ISO 15472 standard. The estimated accuracy of the reported binding energy values is  $\pm 0.2$  eV. Detailed spectra used for quantitative analysis and study of the chemical

environment of the sample components were recorded in the Constant Analyser Energy mode (pass energy: 30 eV, resolution: around 1 eV). Powder samples were pressed into pellets before mounting on standard Omicron sample plates. As the samples were insulating materials, considerable charging was observed during the measurements. Dealing with silicate materials, generally the C 1s line is used for compensation of the charging effect.<sup>[40]</sup> Accordingly, in the present study the lowest binding energy component of the C 1s spectrum, arising from hydrocarbons at 285.0 eV, was selected as reference point. With this calibration reasonable binding energy values were obtained for both Si 2p electrons around 103 eV and Mg 2p electrons around 50.5 eV. The measured spectra were processed by fitting Gaussian-Lorentzian product peaks to the data with the CasaXPS software package<sup>[6]</sup> after removal of Shirley or linear background. Quantitative evaluation of the XPS data was performed by using the XPS MultiQuant software package,<sup>[56,57]</sup> during which homogeneous depth distribution was assumed for all components.

The Nicolet Impact Type 400 FT-IR spectrometer was used for the determination of the adsorbed Py and  $\text{CDCl}_3$  molecules. All of the spectra were recorded at room temperature either with or without adsorptive in the cell. The difference spectra were obtained from the difference between the spectrum of a wafer containing  $\text{CDCl}_3$  or Py and the spectrum of a wafer without adsorptive. Spectra were recorded as an average of 64 scans using a resolution of 2  $\text{cm}^{-1}$ . (For experimental details confer the legends of Figure 3 and Figure S6.)

Catalytic ETB reactions were carried out at atmospheric pressure in a fixed-bed, continuous-flow, glass tube (I.D. 8 mm) microreactor. In situ in the reactor 1 g of catalyst (particle size 0.315–0.65 mm) was activated in oxygen flow (20  $\text{ml min}^{-1}$ ) for 1 h at 450 °C. The reactor had an evaporation zone kept at 120 °C. Liquid ethanol was introduced into the evaporation zone of the He-flushed reactor using a Gilson 307 HPLC Piston Pump. The catalytic activity of the catalysts were tested with feed composition of 14.7 vol.% ethanol/in He. The effect of the reaction temperature was examined at total flow rate of 30  $\text{ml min}^{-1}$  and weight hourly space velocity (WHSV) = 0.5  $\text{g}_{\text{ethanol}} \cdot \text{g}_{\text{cat}}^{-1} \cdot \text{h}^{-1}$ . The effect of WHSV was tested in flow range of 5–120  $\text{ml min}^{-1}$  and  $\text{WHSV} = 0.08\text{--}2 \text{ g}_{\text{ethanol}} \cdot \text{g}_{\text{cat}}^{-1} \cdot \text{h}^{-1}$ . Testing the most active catalysts the high conversion levels at the low WHSV were achieved by diluting 0.50 g catalyst with 0.50 g inert SiC. In order to prevent condensation of the ethanol and the reaction products, the lines of the reactor system were heated up to 120 °C. The reaction products were analysed by on-line GC (Shimadzu GC-2010). The device is equipped with two FID detectors. One is connected to a Chrompack PLOT Fused Silica column with  $\text{Al}_2\text{O}_3/\text{KCl}$  stationary phase (50 m long, 0.32 mm diameter) for the analysis of hydrocarbon products, while the other is connected to the HP-PLOT–U column (30 m long, 0.32 mm diameter) for the analysis of oxygenates. Ethanol and major products were all calibrated in independent measurements. The conversion was calculated from the difference between the amount of ethanol fed and the amount of unreacted ethanol. The selectivity of each product was calculated from the quotient of the number of carbon atoms in them and the number of carbon atoms in the total product. The carbon balance proved to be more than 95 % accurate in almost all cases.

## Acknowledgements

Thanks is due to the support provided by the European Union and the State of Hungary, co-financed by the European Regional Development Fund in the framework of the project No. VEKOP-2.3.2-16-2017-00013.

## Conflict of Interest

The authors declare no conflict of interest.

**Keywords:** Biobutadiene · C–C coupling · Heterogeneous catalysis · Meerwein-Ponndorf-Verley (MPV) type hydrogen transfer · MgO–SiO<sub>2</sub> catalysts

- [1] C. Angelici, B. M. Weckhuysen, P. C. A. Bruijninx, *ChemSusChem* **2013**, *6*, 1595–1614.
- [2] E. V. Makshina, M. Dusselier, W. Janssens, J. Degreève, P. A. Jacobs, B. F. Sels, *Chem. Soc. Rev.* **2014**, *43*, 7917–7953.
- [3] S. V. Lebedev, *J. Gen. Chim.* **1933**, *3*, 698–708.
- [4] J. Ostromislski, *J. Russ. Phys. Chem. Soc.* **1915**, *47*, 1472–1506.
- [5] T. De Baerdemaeker, M. Feyen, U. Müller, B. Yilmaz, F.-S. Xiao, W. Zhang, T. Yokoi, X. Bao, H. Gies, D. E. De Vos, *ACS Catal.* **2015**, *5*, 3393–3397.
- [6] N. Fairley, “CasaXPS software package,” can be found under [www.casaxps.com](http://www.casaxps.com), **2006**
- [7] G. Pomalaza, G. Vofo, M. Capron, F. Dumeignil, *Green Chem.* **2018**, *20*, 3203–3209.
- [8] P. Tu, B. Xue, Y. Tong, J. Zhou, Y. He, Y. Cheng, J. Ni, X. Li, *ChemistrySelect* **2020**, *5*, 7258–7266.
- [9] Y. Xu, Z. Liu, Z. Han, M. Zhang, *RSC Adv.* **2017**, *7*, 7140–7149.
- [10] A. Klein, K. Keisers, R. Palkovits, *Appl. Catal. A* **2016**, *514*, 192–202.
- [11] S. Shylesh, A. A. Gokhale, C. D. Scown, D. Kim, C. R. Ho, A. T. Bell, *ChemSusChem* **2016**, *9*, 1462–1472.
- [12] X. Huang, Y. Men, J. Wang, W. An, Y. Wang, *Catal. Sci. Technol.* **2017**, *7*, 168–180.
- [13] S. Da Ros, M. D. Jones, D. Mattia, M. Schwaab, F. B. Noronha, J. C. Pinto, *Appl. Catal. A* **2017**, *530*, 37–47.
- [14] S.-H. Chung, C. Angelici, S. O. M. Hinterding, M. Weingarh, M. Baldus, K. Houben, B. M. Weckhuysen, P. C. A. Bruijninx, *ACS Catal.* **2016**, *6*, 4034–4045.
- [15] B. Szabó, G. Novodárszki, Z. May, J. Valyon, J. Hancsók, R. Barthos, *Mol. Catal.* **2020**, *491*, 110984.
- [16] H. Niiyama, S. Morii, E. Echigoya, *Bull. Chem. Soc. Jpn.* **1972**, *45*, 655–659.
- [17] X. Wang, Y. Men, J. Wang, S. Liu, Q. Song, M. Yang, *Appl. Catal. A* **2020**, *598*, 117565.
- [18] S. Li, Y. Men, J. Wang, S. Liu, X. Wang, F. Ji, S. Chai, Q. Song, *Appl. Catal. A* **2019**, *577*, 1–9.
- [19] C. Angelici, F. Meirer, A. M. J. Van Der Eerden, H. L. Schaink, A. Goryachev, J. P. Hofmann, E. J. M. Hensen, B. M. Weckhuysen, P. C. A. Bruijninx, *ACS Catal.* **2015**, *5*, 6005–6015.
- [20] C. Angelici, M. E. Z. Velthoen, B. M. Weckhuysen, P. C. A. Bruijninx, *Catal. Sci. Technol.* **2015**, *5*, 2869–2879.
- [21] M. Zhang, M. Gao, J. Chen, Y. Yu, *RSC Adv.* **2015**, *5*, 25959–25966.
- [22] J. V. Ochoa, C. Bandinelli, O. Vozniuk, A. Chierigato, A. Malmusi, C. Recchi, F. Cavani, *Green Chem.* **2016**, *18*, 1653–1663.
- [23] S. Da Ros, M. D. Jones, D. Mattia, J. C. Pinto, M. Schwaab, F. B. Noronha, S. A. Kondrat, T. C. Clarke, S. H. Taylor, *ChemCatChem* **2016**, *8*, 2376–2386.
- [24] O. V. Larina, P. I. Kyriienko, S. O. Soloviev, *Catal. Lett.* **2015**, *145*, 1162–1168.
- [25] Y. Sekiguchi, S. Akiyama, W. Urakawa, T. Koyama, A. Miyaji, K. Motokura, T. Baba, *Catal. Commun.* **2015**, *68*, 20–24.
- [26] M. Lewandowski, G. S. Babu, M. Vezzoli, M. D. Jones, R. E. Owen, D. Mattia, P. Plucinski, E. Mikolajska, A. Ochendusko, D. C. Apperley, *Catal. Commun.* **2014**, *49*, 25–28.
- [27] P. I. Kyriienko, O. V. Larina, S. O. Soloviev, S. M. Orlyk, C. Calers, S. Dzwigaj, *ACS Sustainable Chem. Eng.* **2017**, *5*, 2075–2083.
- [28] V. L. Sushkevich, I. I. Ivanova, *ChemSusChem* **2016**, *9*, 2216–2225.
- [29] J. V. Ochoa, A. Malmusi, C. Recchi, F. Cavani, *ChemCatChem* **2017**, *9*, 2128–2135.
- [30] G. Pomalaza, P. Simon, A. Addad, M. Capron, F. Dumeignil, *Green Chem.* **2020**, *22*, 2558–2574.
- [31] A. D. Patel, K. Meesters, H. Den Uil, E. De Jong, K. Blok, M. K. Patel, *Energy Environ. Sci.* **2012**, *5*, 8430–8444.
- [32] Q. Zhu, B. Wang, T. Tan, *ACS Sustainable Chem. Eng.* **2017**, *5*, 722–733.
- [33] C. D. Wagner, D. E. Passoja, H. F. Hillery, T. G. Kinisky, H. A. Six, W. T. Jansen, J. A. Taylor, *J. Vac. Sci. Technol.* **1982**, *21*, 933–944.
- [34] A. R. González-Elipe, J. P. Espinós, G. Munuera, J. Sanz, J. M. Serratos, *J. Phys. Chem.* **1988**, *92*, 3471–3476.
- [35] C. D. Wagner, A. V. Naumkin, A. Kraut-Vass, J. W. Allison, C. J. Powell, J. R. Rumble Jr, *Natl. Inst. Stand. Technol. Gaithersbg.* **2003**, DOI 10.18434/T4T88 K.
- [36] J. H. Kwak, J. Z. Hu, R. V. F. Turcu, K. M. Rosso, E. S. Ilton, C. Wang, J. A. Sears, M. H. Engelhard, A. R. Felmy, D. W. Hoyt, *Int. J. Greenhouse Gas Control* **2011**, *5*, 1081–1092.
- [37] S. Kvisle, A. Agüero, R. P. A. Sneed, *Appl. Catal.* **1988**, *43*, 117–131.
- [38] A. O. Menezes, P. S. Silva, E. P. Hernández, L. E. P. Borges, M. A. Fraga, *Langmuir* **2010**, *26*, 3382–3387.
- [39] Y. Hayashi, S. Akiyama, A. Miyaji, Y. Sekiguchi, Y. Sakamoto, A. Shiga, T. Koyama, K. Motokura, T. Baba, *Phys. Chem. Chem. Phys.* **2016**, *18*, 25191–25209.
- [40] C. Elmi, S. Guggenheim, R. Gieré, *Clays Clay Miner.* **2016**, *64*, 537–551.
- [41] S. Ardizzone, C. L. Bianchi, M. Fadoni, B. Vercelli, *Appl. Surf. Sci.* **1997**, *119*, 253–259.
- [42] P. Casey, G. Hughes, *J. Appl. Phys.* **2010**, *107*, 074107.
- [43] P. Casey, E. O’Connor, R. Long, B. Brennan, S. A. Krasnikov, D. O’Connell, P. K. Hurley, G. Hughes, *Microelectron. Eng.* **2009**, *86*, 1711–1714.
- [44] A. Chakradhar, U. Burghaus, *Surf. Sci.* **2013**, *616*, 171–177.
- [45] E. A. Paukshtis, N. S. Kotsarenko, L. G. Karakchiev, *React. Kinet. Catal. Lett.* **1979**, *12*, 315–319.
- [46] H. Y. Luo, D. F. Consoli, W. R. Gunther, Y. Román-Leshkov, *J. Catal.* **2014**, *320*, 198–207.
- [47] G. Chuah, S. Jaenicke, Y. Zhu, S. Liu, *Curr. Org. Chem.* **2006**, *10*, 1639–1654.
- [48] H. Niiyama, E. Echigoya, *Bull. Chem. Soc. Jpn.* **1972**, *44*, 938–939.
- [49] A. Chierigato, J. V. Ochoa, C. Bandinelli, G. Fornasari, F. Cavani, M. Mella, *ChemSusChem* **2015**, *8*, 377–388.
- [50] V. V. Ordonsky, V. L. Sushkevich, I. I. Ivanova, *J. Mol. Catal. A* **2010**, *333*, 85–93.
- [51] J. Scalbert, F. Thibault-Starzyk, R. Jacquot, D. Morvan, F. Meunier, *J. Catal.* **2014**, *311*, 28–32.
- [52] R. P. Eischens, W. A. Pliskin, M. J. D. Low, *J. Catal.* **1962**, *1*, 180–191.
- [53] H. Zhang, M. Y. S. Ibrahim, D. W. Flaherty, *J. Catal.* **2018**, *361*, 290–302.
- [54] R. G. Pearson, *J. Am. Chem. Soc.* **1985**, *107*, 6801–6806.
- [55] R. G. Pearson in *Chemical Hardness*, Wiley-VCH Verlag GmbH, Weinheim, **2005**, pp. 1–28.
- [56] M. Mohai, *Surf. Interface Anal.* **2004**, *36*, 828–832.
- [57] M. Mohai, *XPS MultiQuant: Multi-Model X-Ray Photoelectron Spectroscopy Quantification Program 3.00.16*, **2003**.

Manuscript received: June 17, 2020  
Revised manuscript received: August 17, 2020  
Accepted manuscript online: August 18, 2020  
Version of record online: September 16, 2020